# A Semi-parametric Model of the Hemodynamic Response for Multi-Subject fMRI Data

Tingting Zhang[a,1], Fan Li[b], Lane Beckes[c], James A. Coan[c,1]

[a]*Department of Statistics, University of Virginia, Charlottesville, VA 22904, USA*
[b]*Department of Statistical Science, Duke University, Durham, NC 27708, USA*
[c]*Department of Psychology, University of Virginia, Charlottesville, VA 22904, USA*

**Abstract**

A semi-parametric model for estimating hemodynamic response function (HRF) from multi-subject fMRI data is introduced within the context of the General Linear Model. The new model assumes that the HRFs for a fixed brain voxel under a given stimulus share the same unknown functional form across subjects, but differ in height, time to peak, and width. A nonparametric spline-smoothing method is developed to evaluate this common functional form, based on which subject-specific characteristics of the HRFs can be estimated. This semi-parametric model explicitly characterizes the common properties shared across subjects and is flexible in describing various brain hemodynamic activities across different regions and stimuli. In addition, the temporal differentiability of the employed spline basis enables an easy-to-compute way of evaluating latency and width differences in hemodynamic activity. The proposed method is applied to data collected as part of an ongoing study of socially mediated emotion regulation. Comparison with several existing methods is conducted through simulations and real data analysis.

*Keywords:* hemodynamic response function, fMRI, GLM, multi-subject, regularization, smoothing, spline.

[1]Corresponding author at: Halsey Hall 111, University of Virginia, Charlottesville, VA, 22904, USA. Fax: (434) 924-3076. E-mail address: tz3b@virginia.edu (Tingting Zhang); or 102 Gilmer Hall, PO Box 400400, University of Virginia, Charlottesville, VA, 22904, USA. Email: jcoan@virginia.edu (James Coan)

## 1. Introduction

Functional magnetic resonance imaging (fMRI) measures brain activity through monitoring blood oxygen level dependent (BOLD) contrasts between two or more experimental conditions − an approach that requires the ability to track changes in blood flow with high spatial resolution (Ogawa et al., 1992). BOLD imaging has played a major role in neuropsychological experiments designed to associate various psychological phenomena with specific regions or circuits of the brain. Complex, multi-subject fMRI designs involving multisensory stimuli are growing more common. Such designs are very informative for investigating brain activity across different regions, stimuli, and subjects. But complex experimental designs also introduce nontrivial challenges for joint modelling, analysis, and computation of BOLD imaging data.

A widely-used framework for analyzing fMRI data is the General Linear Model (GLM) (Friston et al., 1995a; Friston et al., 1995b; Worsley and Friston, 1995), where the observed BOLD time series are modeled as a convolution of the experimentally-designed stimulus paradigm and the hemodynamic response function (HRF). The key to analysis lies in estimating the HRF. Within the framework of the GLM, estimation methods differ in their assumptions about the shape of the HRF. Parametric approaches, which assume the HRF follows a known functional form with a number of free parameters, include the canonical form of mixtures of gamma functions (Friston et al. 1998; Glover 1999; Worsley et al. 2002), poisson function (Friston et al., 1994), inverse logit function (Lindquist and Wager, 2007) and radial basis functions (Riera et al., 2004). When the underlying HRF deviates from the assumed functional form, however, parametric methods may be inadequate. By contrast, nonparametric approaches make no explicit assumptions about the functional form of the HRF. These include methods that represent the HRF with a linear combination of functional bases (Aguirre et al., 1998; Zarahn, 2002; Woolrich et al., 2004; Vakorin et al., 2007), and methods that treat the HRF at every time point as a free parameter (Dale, 1999; Lange et al., 1999). Ultimately, nonparametric methods allow for more flexibility in accommodating the variability in brain activity across stimuli, brain regions and individ-

uals.

Since nonparametric methods usually involve a large number of free parameters and the HRFs are generally believed to be smooth (Buxton et al., 2004), smoothing techniques such as kernel smoothing and regularization are commonly employed. For example, the smooth finite impulse response (SFIR) method (Glover, 1999; Goutte et al., 2000; Ollinger et al., 2001) exploits a regularization term to obtain smooth HRF estimates that satisfy a boundary condition. Vakorin et al. (2007) and Zhang et al. (2007) fitted the HRF by spline bases, and used Tikhonov regularization to achieve smoothness. More recently, Casanova et al. (2008, 2009) combined Tikhonov regularization and generalized cross validation (Tik-GCV) to improve the computation. Strategies that combine kernel smoothing and Tikhonov regularization (BTik-Kern) have also been developed (Zhang et al., 2012).

In analyzing multi-subject fMRI data, standard approaches apply a selected method − one of the above, for example − to each subject's data independently to account for the variability across subjects (e.g., Aguirre et al., 1998; Handwerker et al., 2004). Intuitively, exploiting population-wide common characteristics may improve the HRF estimation, especially when the data from each individual have a low signal-to-noise ratio (SNR). One way to achieve this is to develop mixed-effect and random-effect models (Friston et al., 1999; Mumford and Nichols, 2006). Another way is to explicitly assume that the HRFs of different subjects in a population have a similar shape. For example, Friston et al. (1998), Liao et al. (2002) and Henson et al. (2002) used Taylor expansion to evaluate subject-specific magnitudes and latencies with a fixed canonical HRF shape. Zhang et al. (2012) used the sample-averaged HRF to conduct bias correction for the Tikhonov-regularized nonparametric estimator. However, the former approach does not readily accommodate the variability in the HRF shapes across different brain areas and stimuli, while the latter produces well-performing estimates mainly when the difference in the magnitude accounts for most variation in the HRFs across subjects.

The GLM can be viewed as a special case of the generalized functional linear model (GFLM, Ramsay and Silverman, 2005), where the functional parameters of interest are

the HRFs. Despite the vast statistical literature on GFLM (Müller and Stadtmüller, 2005; Yao, Müller, and Wang, 2005; Crainiceanu et al., 2009; Di et al., 2009; Li, Wang and Carroll (2010); to name a few), few of these methods can readily accommodate the unique features of fMRI. In this article, within the framework of the GLM, we propose a novel semi-parametric model for multi-subject fMRI data, assuming that the HRFs for a fixed brain voxel associated with a given stimulus share a common but unknown functional form across subjects, but differ in height, time to peak, and width. We use nonparametric spline expansions (Eubank, 1988; Wahba, 1990; De Boor, 2001; Ruppert et al., 2003) to estimate this functional form. This semi-parametric model explicitly characterizes the common properties shared across subjects and is highly flexible in describing various brain hemodynamic activities across different regions and stimuli. In addition, we develop a new fast-to-compute algorithm for model estimation that is scalable to large-scale multi-subject fMRI data.

The rest of the article is organized as follows. In Section 2, we first propose the semi-parametric model for the HRFs from multi-subject data, then introduce the estimation method based on spline-basis expansion. A fast algorithm to choose the key tuning parameters is also developed. In Section 3, we compare the proposed method with several existing methods via simulated data and apply it to the fMRI data collected during a social emotion regulation experiment involving threat and safety stimuli while alone or during hand holding by friends and strangers (cf., Coan, Beckes, and Allen, 2012). Section 4 concludes with a brief discussion.

## 2. Materials and Methods

### *2.1. A General Semi-parametric Model for HRF*

Let $y_i(t)$ for $t = \delta, \cdots, T \cdot \delta$ and $i = 1, \cdots, n$ be the observed fMRI time series of a given brain voxel of subject $i$, where $\delta$ is the experiment time unit when each 3D scan is

captured. In most experiments, $\delta$ ranges from 0.5 to 2 seconds. The GLM is

$$y_i(t) = X_i(t) \cdot d_i + \sum_{k=1}^{K} \int_0^m h_{i,k}(u) \cdot v_{i,k}(t-u)du + \varepsilon_i(t), \tag{1}$$

where $X_i(t) \in \Re^p$ is a vector of time-varying covariates, $v_{i,k}(t-u)$ are known functions, $m$ is a fixed constant, and $\varepsilon_i(t)$ is an error term. The HRF $h_{i,k}(u)$ describes the brain response of subject $i$ to the $k$th stimulus in a given region, and the research interest lies in estimating $h_{i,k}(u)$ for all $i, k$. In fMRI studies, the $v_{i,k}(t)$ is called stimulus function, which characterizes the experiment for subject $i$ under the $k$th stimulus: $v_{i,k}(t) = 1$ if the $k$th stimulus is evoked at time $t$; otherwise, it equals 0. The covariates $X_i(t)$ characterize the BOLD signal from other known sources, such as respiration and heartbeat. Usually, the $X_i(t) \cdot d_i$ is a low-order polynomial of $t$ modelling the low-frequency drift due to physiological noise or subject motion. Following the common practice in the literature (Smith et al., 1999; Brosch, et al., 2002; Luo and Puthusserypady, 2008), we assume $X_i(t) = (1, t, t^2)$ with the drifting parameters $d_i = (d_{0,i}, d_{1,i}, d_{2,i})'$.

Here we propose a flexible semi-parametric model for the HRF that efficiently utilizes the multi-subject information. We assume the HRFs for a fixed voxel under stimulus $k$, the $h_{i,k}$'s, share a common functional form but differ in magnitude and latency across subjects, as follows,

$$h_{i,k}(t) = A_{i,k} \cdot f_k(t + D_{i,k}), \tag{2}$$

where $A_{i,k}$ and $D_{i,k}$ represent magnitude and latency of the chosen voxel's reaction to the $k$th stimulus of subject $i$, respectively. The function $f_k(t)$ can be viewed as the population-average HRF. No parametric assumption of $f_k(t)$ except differentiability is imposed, distinct from the proposal by Friston et al. (1998) and Henson et al. (2002) where $f_k(t)$ is fixed as the canonical HRF. Model (2) has two major advantages: first, by assuming all the subjects have a common functional form of the HRF it enables "borrowing" information across subjects while allowing for subject-specific characteristics; second, the

nonparametric nature of $f_k(t)$ provides maximum flexibility in modelling heterogenous brain activities across regions and stimuli.

We note that a shape-invariant model similar to (2) has been proposed before for longitudinal data analysis (Lindstrom, 1995; Ladd and Lindstrom, 2000). However, the different contexts lead to fundamental distinctions in inference and computation between these works and ours. First, in the GLM for fMRI data, the mean outcome is a sum of convolutions of HRFs with associated stimuli, and there are no direct observations from the target functions (the HRFs). The models used for standard longitudinal data analysis, on the other hand, do not involve convolutions and deal with only observed data, making the estimation more straightforward. Second, our model allows multiple HRFs in possibly distinct shapes to account for different stimulus effects, while models in standard functional data analysis, including the aforementioned ones typically only allow one shape-invariant function. Third, as fMRI data usually contain thousands to hundreds of thousands time series for each subject as opposed to tens to hundreds in standard longitudinal data, computation is much more challenging in the former and new computational algorithms need to be developed.

Model (2) only considers differences in magnitude and latency across subjects. To accommodate the variation of the functional width $W_{i,k}$, which measures the duration of brain activity, we will also investigate the following extension:

$$h_{i,k}(t) \quad = \quad A_{i,k} \cdot f_k \left( \frac{t + D_{i,k}}{W_{i,k}} \right). \tag{3}$$

*2.2. Parameter Estimation via Spline*

We propose an estimation strategy for model (2) using spline-basis expansions. Spline-based methods have been widely used in functional representation and estimation, where a model with parameter functions becomes a generalized linear model with scalar parameters (basis coefficients). Overfitting can be overcame through basis selection or penalization (for details see Eubank, 1988; Parker and Rice, 1985; Wahba, 1990; Green and Silverman, 1994; and Ramsay and Silverman, 2005). However, these methods are only

applicable for estimating each subject's HRFs independently without accounting for the population-wide common structure. The proposed strategy here aims at incorporating both population-wide and subject-specific characteristics into the estimation procedure simultaneously, which is more efficient but also more challenging in computation.

As the latency $D_{i,k}$ is usually much smaller than the experimental time unit, the non-linear model (2) is first converted to a linear one by using first-order Taylor expansion:

$$h_{i,k}(t) \approx A_{i,k} \cdot f_k(t) + C_{i,k} \cdot f_k^{(1)}(t), \tag{4}$$

where $C_{i,k} = A_{i,k} \cdot D_{i,k}$, and $f_k^{(1)}$ denotes the 1st derivative of $f_k$ (from now on we will use the superscript $^{(j)}$ to denote the $j$th derivative of a function). We then represent $f_k(t)$ by *cubic B-spline basis*: $f_k(t) = \sum_{l=1}^{L} a_{l,k} b_l(t)$, where the basis functions $b_l(t)$ are chosen based on a partition $\Pi_q = (t_0 = 0, t_1, \cdots, t_q = m)$ of the interval $[0, m]$. Selection of the knots $\Pi_q$ is discussed later. Given the boundary condition $h_{i,k}(0) = h_{i,k}(m) = 0$, we let $a_{1,k} = a_{L,k} = 0$. Then model (1) is reduced to a bilinear one:

$$y_i(t) = X_i(t) \cdot d_i + \sum_{k=1}^{K} \sum_{l=2}^{L-1} (A_{i,k} \cdot a_{l,k}) \rho_{l,k}^i(t) + \sum_{k=1}^{K} \sum_{l=2}^{L-1} (C_{i,k} \cdot a_{l,k}) \varrho_{l,k}^i(t) + \varepsilon_i(t), \tag{5}$$

where $\rho_{l,k}^i(t) = \int_0^m b_l(u) v_{i,k}(t-u) du$ and $\varrho_{l,k}^i(t) = \int_0^m b_l^{(1)}(u) v_{i,k}(t-u) du$ are known functions. Here $A_{i,k}$, $C_{i,k}$ and $a_{l,k}$ are not directly identifiable, but $\omega_{l,k}^i = A_{i,k} \cdot a_{l,k}$ and $\nu_{l,k}^i = C_{i,k} \cdot a_{l,k}$ are unique. Thus, identifiability can be achieved, for example, by forcing the average of the estimates of $A_{i,k}$, $\sum_{i=1}^{n} \hat{A}_{i,k}/n$, to be 1 for all $k$.

Let $\Theta$ denote all the parameters involved in model (5), it can be estimated by minimizing the mean squared error (MSE) of $y_i(t)$: $\hat{\Theta} = \arg\min_{\Theta} \text{MSE}(\Theta)$, where

$$\text{MSE}(\Theta) = \frac{1}{n} \sum_{i=1}^{n} \sum_{t=\delta}^{T \cdot \delta} \left\{ y_i(t) - X_i(t) \cdot d_i - \sum_{k=1}^{K} \sum_{l=2}^{L-1} (A_{i,k} \cdot a_{l,k}) \rho_{l,k}^i(t) - \sum_{k=1}^{K} \sum_{l=2}^{L-1} (C_{i,k} \cdot a_{l,k}) \varrho_{l,k}^i(t) \right\}^2.$$

A standard approach to minimizing $\text{MSE}(\Theta)$ is through alternating least squares algo-

| parameter | description |
|---|---|
| $X_i(t)$ | a vector of known time-varying covariates |
| $d_i$ | coefficients for $X_i(t)$ |
| $A_{i,k}$ | subject-specific magnitude of the $k$th HRF |
| $D_{i,k}$ | subject-specific latency of the $k$th HRF |
| $W_{i,k}$ | subject-specific width of the $k$th HRF |
| $C_{i,k}$ | product $A_{i,k} \cdot D_{i,k}$ |
| $E_{i,k}$ | product $-A_{i,k} \cdot (W_{i,k} - 1)$ |
| $a_{l,k}$ | coefficients of the spline bases representing the $k$th common function $f_k(t)$ |
| $\omega^i_{l,k}$ | $A_{i,k} \cdot a_{l,k}$ also coefficient of the spline basis $b_l(t)$ in $h_{i,k}(t) = \sum_{l=2}^{L-1} \omega^i_{l,k} b_l(t)$ |
| $\nu^i_{l,k}$ | product $C_{i,k} \cdot a_{l,k}$ |
| $\rho^i_{l,k}(t)$ | known functions $\int_0^m b_l(u) v_{i,k}(t-u) du$ |
| $\varrho^i_{l,k}(t)$ | known functions $\int_0^m b_l^{(1)}(u) v_{i,k}(t-u) du$ |

Table 1: Notations of key parameters

rithm, iterating between the following two steps: (a) given the estimates of $\Delta = (a_{l,k}; l = 2, \ldots, L, k = 1, \ldots, K)$, solve for the ordinary least square (OLS) estimates of $\Psi = (d_i,\ A_{i,k},\ C_{i,k}; i = 1, \ldots, n, k = 1, \ldots, K)$ in model (5); (b) given the estimates of $\Psi$, solve for the OLS estimates of $\Delta$. However, computation of this approach involves expensive iterations of matrix inversion and transformation, letting alone the issue of knot selection of $\Pi_q$. Instead, we propose an algorithm that avoids knot selection and iterative procedure by imposing a penalty on the roughness of the HRFs, as follows:

(i) Start with a large number of equally-spaced knots such that the number of free parameters $\omega^i_{l,k}$ in (5), $K \cdot (L-2)$, is comparable to but smaller than the number of observations $T$.

(ii) For each subject $i$, set $\nu^i_{l,k} = 0$ so that $h_{i,k}(t) = \sum_{l=2}^{L-1} \omega^i_{l,k} b_l(t)$ in model (5). Then given a pre-specified penalty parameter $\lambda (> 0)$, obtain the parameter estimates $\hat{d}_i$ and $\hat{\omega}^i_{l,k}$ by minimizing

$$\sum_{t=\delta}^{T\cdot\delta} \left\{ y_i(t) - X_i(t) \cdot d_i - \sum_{k=1}^{K} \sum_{l=2}^{L-1} \omega^i_{l,k} \cdot \rho^i_{l,k}(t) \right\}^2 + \lambda \cdot \sum_{k=1}^{K} \int_0^m \left\{ h^{(2)}_{i,k}(u) \right\}^2 du, \qquad (6)$$

where $\int_0^m \left\{h_{i,k}^{(2)}(u)\right\}^2 du = \int_0^m \left\{\sum_{l=2}^{L-1} \omega_{l,k}^i b_l^{(2)}(u)\right\}^2 du$.

(iii) Estimate $a_{l,k}$ by $\hat{a}_{l,k} = \sum_{i=1}^n \hat{\omega}_{l,k}^i / n$.

(iv) Given $\hat{a}_{l,k}$ for all $l, k$ from (iii), solve for the OLS estimate $(\hat{d}_i, \hat{A}_{i,k}, \hat{C}_{i,k})$ for all $i, k$ in model (5).

Upon obtaining the parameter estimates, we estimate the HRFs by $\hat{h}_{i,k}(t) = \hat{A}_{i,k}\hat{f}_k(t) + \hat{C}_{i,k}\hat{f}_k^{(1)}(t)$, where $\hat{f}_k(t) = \sum_{l=2}^{L-1} \hat{a}_{l,k} b_l(t)$. The summary statistics, height (HR), time to peak (TTP) and width (W), respectively characterizing the magnitude, reaction time and duration of brain response to the $k$th stimulus of $i$th subject are extracted based on $\hat{h}_{i,k}(t)$ through procedures described in Lindquist and Wager (2007).

Step (ii) is equivalent to estimating each subject's HRFs independently with each $h_{i,k}(t)$ represented by the given set of spline basis in a fully nonparametric manner, and Step (iii) is to take the average of these nonparametric HRF estimates as the estimate of $f_k(t)$, based on which subject-specific parameters $A_{i,k}$ and $C_{i,k}$ are reevaluated in Step (iv). Besides simplifying the calculation, there are two reasons justifying evaluating $f_k(t)$ by the average of independent estimates of $h_{i,k}(t)$: first, by assuming population-average latency $\mathbb{E}(D_{i,k})$ to be zero for all $k$ without loss of generality, $D_{i,k}$ can be considered averaged out close to zero with large enough $n$ in estimating $f_k(t)$—population mean of $h_{i,k}(t)$; second, the estimate of $a_{l,k}$ should depend little on the value of $\nu_{l,k}^i$, which is much smaller than $\omega_{l,k}^i$, if $D_{i,k}$ is much smaller than the time unit.

In Step (ii), the penalization on the integral of squared second derivatives of the HRFs is used to control the roughness of the estimate. A similar strategy is adopted in Marrelec et al. (2001, 2003). To solve for (6), we first convert model (1) with the representation $h_{i,k}(t) = \sum_{l=2}^{L-1} \omega_{l,k}^i b_l(t)$ to a matrix form as

$$Y_i = \Lambda_i \cdot \eta_i + \boldsymbol{\varepsilon}_i, \tag{7}$$

where $Y_i = (y_i(1), \ldots, y_i(T))'$, $\eta_i = (d_i', \omega_{2,1}^i, \ldots, \omega_{L-1,K}^i)'$, $\boldsymbol{\varepsilon}_i = (\varepsilon_i(1), \ldots, \varepsilon_i(T))'$, and $\Lambda_i$ is the design matrix composed of $X_i$ and $\rho_{l,k}^i(t)$ for all $k$ and $l$. Let $P$ be a $(3 + (L-2) \cdot$

$K) \times (3 + (L-2) \cdot K)$ matrix whose first three rows and three columns are zeros, and the $(2 + l + (k-1)(L-2), 2 + \tilde{l} + (k-1)(L-2))$ entry equals $\int_0^m \int_0^m b_l^{(2)}(u) b_{\tilde{l}}^{(2)}(\tilde{u}) du d\tilde{u}$ for $l, \tilde{l} = 2, \ldots, L-1$ and $k = 1, \ldots, K$. Penalizing the roughness of the HRF estimates characterized by $\int_0^m \left\{ h_{i,k}^{(2)}(u) \right\}^2 du$ is equivalent to regularizing the estimate of $\eta_i$ by $P$ in linear regression. Therefore, the optimizer $\eta_i$ of expression (6) for a fixed $\lambda$ is given by

$$\hat{\eta}_i = (\Lambda_i' \Lambda_i + \lambda \cdot P)^{-1} \Lambda_i' \cdot Y_i. \tag{8}$$

For the more flexible model (3), since $W_{i,k}$ is usually close to 1, we will again use Taylor expansion to approximate:

$$h_{i,k}(t) \approx A_{i,k} \cdot f_k(t) + A_{i,k} \cdot D_{i,k} \cdot f_k^{(1)}(t) - A_{i,k} \cdot (W_{i,k} - 1) f_k^{(1)}(t) \cdot t.$$

Similar spline-basis-based estimation strategy as above can be developed to estimate the parameters, with Step (iv) being modified to

(iv)* Given $\hat{a}_{l,k}$ for all $l, k$ from (iii), solve for the ordinary least square (OLS) estimate of $\Psi = (d_i, A_{i,k}, C_{i,k}, E_{i,k})$, where $E_{i,k} = -A_{i,k} \cdot (W_{i,k} - 1)$ for all $i, k$ in model (3).

Then $h_{i,k}(t)$ is estimated by $\hat{h}_{i,k}(t) = \hat{A}_{i,k} \hat{f}_k(t) + \hat{C}_{i,k} \hat{f}_k^{(1)}(t) + \hat{E}_{i,k} \hat{f}_k^{(1)}(t) \cdot t$, and the estimates of HR, TTP, and W are obtained in the same manner as above. The key notations above are summarized in Table 1.

### *2.3. Algorithm for Selecting Penalty Parameter*

The penalty parameter $\lambda$ controls the balance between the fitting error and the smoothness of the estimated function form. Ordinary cross-validation (OCV) and generalized cross-validation (GCV, Wahba, 1990) are standard methods for choosing the penalty parameter for Tikhonov-regularized estimates. In the context of functional data analysis, Reiss and Ogden (2007, 2009) proposed selection procedures based on GCV, as well as restricted maximum likelihood (REML), which is also investigated in Wood (2011). In general, OCV is time consuming, especially for data with a large number of voxels, while

the GCV and REML-based methods are designed to select the optimal $\lambda$ for estimating individual $h_{i,k}(t)$ instead of the aggregated function $f_k(t)$. Since the ultimate goal of using penalization in Step (ii) is to obtain sample-averaged estimate $\hat{f}_k(t)$, we propose an alternative computationally efficient algorithm for evaluating the average mean squared error (AMSE) of $\hat{a}_{l,k}$, the coefficients of $f_k(t)$, and select the $\lambda$ leading to the smallest estimated AMSE. The analytical details for deriving the mean and variance of $\hat{a}_{l,k}$ as functions of $\lambda$ are given in the Appendix. The estimation algorithm is as follows.

1. Starting from a small $\lambda_0$, say 0.1, obtain the estimate $\hat{\eta}_i^0$ using formula (8) . Based on it, evaluate the variance $\sigma_i^2$ of $\boldsymbol{\varepsilon}_i$ in (7) for each subject $i$ by the model fitting error. Denote the median of the estimated $\sigma_i^2$ by $\hat{\sigma}^2$ and the average of $\hat{\eta}_i^0$ by $\bar{\eta}_0$.

2. For each candidate $\lambda$, calculate the matrices $\Omega_\lambda^i = \Lambda_i'\Lambda_i + \lambda \cdot P$ and $\Omega_0^i = \Lambda_i'\Lambda_i$, and obtain the quantities $r_{k,l}^i$ and $\tau_{k,l}^i$ from

$$\begin{aligned}(d_{0,i}, d_{1,i}, d_{2,i}, r_{1,2}^i, \ldots, r_{1,L-1}^i, r_{2,2}^i, \ldots, r_{K,L-1}^i)' &= \left((\Omega_\lambda^i)^{-1}\Omega_0^i - \mathbf{I}_{3+K\cdot(L-2)}\right)\bar{\eta}_0, \\ (\pi_0^i, \pi_1^i, \pi_2^i, \tau_{1,2}^i, \ldots, \tau_{1,L-1}^i, \tau_{2,2}^i, \ldots, \tau_{K,L-1}^i)' &= \text{diag}\left((\Omega_\lambda^i)^{-1}\Omega_0^i(\Omega_\lambda^i)^{-1}\right)\hat{\sigma}^2.\end{aligned}$$

3. For each candidate $\lambda$, get an estimate of AMSE as

$$\widehat{\text{AMSE}}(\lambda) = \sum_{k=1}^{K}\sum_{l=2}^{L-1}\sum_{i=1}^{n}\tau_{k,l}^i/n^2 + \sum_{k=1}^{K}\sum_{l=2}^{L-1}(\sum_{i=1}^{n} r_{k,l}^i/n)^2.$$

4. Choose the $\lambda$ that minimizes $\widehat{\text{AMSE}}(\lambda)$.

As a large number of coefficients for the basis functions are involved in the estimation, we employed a small penalization in Step 1 to prevent the possible issue of ill-posed matrix inversion and to regularize the variation of the estimates at the cost of a small bias. Computation of the algorithm is of linear order of the number of subjects for each voxel. In practice, instead of selecting the optimal parameter for each voxel, we use one penalty parameter for each region of interest (ROI), which is selected based on the data

from one representative voxel or averaged data of the ROI. Note that the calculation of $\hat{\sigma}^2$ is under the assumption of independent and identically distributed (i.i.d.) error terms $\boldsymbol{\varepsilon}_i$. Simulations show that the proposed parameter selection procedure is robust to deviations from this assumption.

## 3. Results

### *3.1. Simulated data*

**Data Generation.** The simulation study follows the event-related experimental design of the Monetary Incentive Delay (MID) task (Knutson et al., 2000), where 6 stimuli are randomized over a span of 223 frames with occurrence percentages of 12.5%, 18.75%, 18.75%, 12.5%, 18.75%, and 18.75%, respectively. The corresponding six HRFs are simulated from a form similar to model (3): $h_{i,k}(t) = A_{i,k} \cdot \phi_{i,k}((t + D_{i,k})/W_{i,k})$, with the function $\phi_{i,k}(t)$ controlling the shape of the HRF for the $k$th stimulus of the $i$th subject. Following Worsley et al. (2002), $\phi_{i,k}(t)$ is assumed to be the difference of two gamma density functions as follows (the subscript $k$ is dropped here):

$$\phi_i(t) = b_{1,i}^{a_{1,i}} \frac{t^{a_{1,i}-1} \exp(-b_{1,i}t)}{\Gamma(a_{1,i})} - c \cdot b_{2,i}^{a_{2,i}} \frac{t^{a_{2,i}-1} \exp(-b_{2,i}t)}{\Gamma(a_{2,i})}. \tag{9}$$

The parameters for the simulated HRFs are given in Table 2 and examples of the simulated HRFs are displayed in Figure 1. Specifically, the first and the second HRFs follow exactly the canonical form in SPM, only differing in subject-specific magnitude and latency, while the third are added some variation of the duration of brain activity ($W_{i,k}$) across subjects. The range of $W_{i,k}$ is chosen to be not too far from 1 such that the values of $h_{i,k}(t)$ beyond domain $[0, m]$ are close to zero. The fourth and the fifth HRFs follow a functional form distinct from the canonical one, and differ in magnitude, latency and width. The functional shapes for the six HRFs vary across subjects.

Following Casanova et al. (2008), we generated error terms $\varepsilon_i$ from an autoregressive

| $k$ | $A_{i,k}$ | $D_{i,k}$ | $W_{i,k}$ | $a_{1,i}$ | $a_{2,i}$ | $b_{1,i}$ | $b_{2,i}$ | $c$ |
|---|---|---|---|---|---|---|---|---|
| 1 | N(300, $50^2$) | 0 | 1 | 6 | 16 | 1 | 1 | 1/6 |
| 2 | $A_{i,1}$+U(30, 50) | U(-0.2,0.2) | 1 | 6 | 16 | 1 | 1 | 1/6 |
| 3 | $A_{i,2}$ | $D_{i,2}$ | U(0.9, 1.1) | 6 | 16 | 1 | 1 | 1/6 |
| 4 | U(200, 700) | U(-1,1) | 1 | 20 | 22 | 3 | 3 | 2/3 |
| 5 | $A_{i,4}$+U(60, 100) | $D_{i,4}$ | U(0.8,1.2) | 20 | 22 | 3 | 3 | 2/3 |
| 6 | U(300, 800) | 0 | 1 | U(18,22) | U(20,24) | U(3,4) | U(3,4) | 1/6 |

Table 2: Parameters of simulated HRFs $h_{i,k}$, where N($\mu, \sigma^2$) denotes a normal distribution with mean $\mu$ and variance $\sigma^2$, and U$(a, b)$ denotes a uniform distribution with boundary values $a$ and $b$.

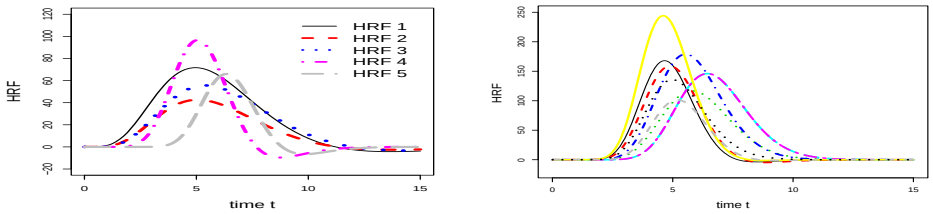


(a) HRF 1 to HRF 5 (b) HRF 6

Figure 1: Examples of simulated HRFs: (a) one simulated HRF for each of stimuli 1 to 5. (b) several simulated HRF 6

model of order 4 (AR(4)) with lag-1 correlation of 0.45 and lag-2 correlation of 0.35:

$$\varepsilon_i(t) = 0.37\,\varepsilon_i(t-1) + 0.14\,\varepsilon_i(t-2) + 0.05\,\varepsilon_i(t-3) + 0.02\,\varepsilon_i(t-4) + e_i(t),$$

where $e_i(t) \overset{i.i.d}{\sim} \text{N}(0, \sigma_i^2)$, and $\sigma_i \sim \text{Gamma}(1, 1/10) + 10$ imitating the heteroscedastic variances across subjects in practice. The SNR defined as $10 \log_{10}\left\{\frac{\text{var(signal)}}{\text{var(noise)}}\right\}$ varied between -3 to 16 with $99\%$ of probability across subjects.

We simulated 100 i.i.d. fMRI data for $n = 19$ subjects, each of which has 223 frames separated by 2s (TR). Within each replicate, we first simulated $n$ sets of random functions $h_{i,k}(t)$ based on the parameters in Table 2, then calculated the convolution of $h_{i,k}(t)$ and the stimulus function as in the GLM (1), and finally obtained the observed fMRI data by adding the generated AR(4) errors and a drifting term to the convolution, with the

drifting parameters being $d_{0,i} \sim \text{U}(-1, 1),\ d_{1,i} \sim \text{U}(-0.1, 0.1),\ d_{2,i} \sim \text{U}(-0.05, 0.05)$. The first four frames were excluded in the data analysis, giving $T = 219$.

**Statistical Analysis and Discussion.** To draw a comparison between the proposed semi-parametric spline method with the existing nonparametric methods, we applied the following methods to estimate the HRFs from the simulated data: the basis set method (Friston et al., 1998) that represents the HRF by a linear combination of the canonical HRF and its temporal derivative (referred to as the canonical method hereafter); SFIR (Goutte et al., 2000); Tik-GCV (Casanova et al., 2008); BTik-Kern (Zhang et al., 2012); and the spline methods based on model (2) and (3), referred to as "Spline" and "Spline-W", respectively.

We used the criterion of average relative error (ARE) for comparison:

$$e(S_k) = \frac{1}{n}\sum_{i=1}^{n}\frac{|S_{i,k} - S_{i,k}^{est}|}{S_{i,k}}, \quad e(\text{RMSE}_k) = \frac{1}{n}\sum_{i=1}^{n}\frac{\parallel h_{i,k} - h_{i,k}^{est} \parallel}{\parallel h_{i,k} \parallel},$$

where $S$ stands for a summary statistic of the HRF, including HR, TTP and W, and RMSE stands for root mean square error, and $\parallel \cdot \parallel$ is the $L^2$ norm.

The median AREs of the HRF estimates in the 100 replicates from different methods are reported in Table 3. Both the spline methods and BTik-Kern outperform Tik-GCV, SFIR (with $g = 1$), and the canonical method, leading to significantly smaller AREs of almost all statistics. The spline methods beat BTik-Kern except in estimating HR and RMSE for the HRFs following the canonical form (HRFs 1-3). Though BTik-Kern also utilizes information across subjects, it does not explicitly model the common functional form $f_k(t)$ and does not impose differentiability on HRFs. This explains its general underperformance comparing to the spline methods. Nevertheless, the bias correction implemented in BTik-Kern using sample-averaged data is most effective in gaining efficiency when the HRFs mainly differ in magnitude, as evident from the smaller AREs for the first three HRFs. This advantage diminishes when the difference in magnitude is not the major source of the variability in the HRFs across subjects, as in HRFs 4-6. Readers are referred to Zhang et al. (2012) for detailed comparison between BTik-Kern and the other

| | HRF $k$ | Spline | Spline-W | BTik-Kern | Tik-GCV | SFIR | Canonical |
|---|---|---|---|---|---|---|---|
| HR | 1 | 0.43 | 0.42 | 0.42 | 0.49 | 0.71 | 0.75 |
| | 2 | 0.42 | 0.40 | 0.27 | 0.44 | 0.74 | 0.70 |
| | 3 | 0.39 | 0.35 | 0.25 | 0.44 | 0.36 | 0.85 |
| | 4 | 0.30 | 0.33 | 0.50 | 0.62 | 0.75 | 0.74 |
| | 5 | 0.32 | 0.34 | 0.44 | 0.59 | 0.72 | 0.83 |
| | 6 | 0.20 | 0.19 | 0.43 | 0.60 | 0.63 | 0.87 |
| TTP | 1 | 0.15 | 0.16 | 0.30 | 0.43 | 0.77 | 0.35 |
| | 2 | 0.12 | 0.13 | 0.11 | 0.32 | 0.56 | 0.56 |
| | 3 | 0.12 | 0.13 | 0.24 | 0.44 | 0.48 | 0.50 |
| | 4 | 0.05 | 0.07 | 0.10 | 0.60 | 0.49 | 0.42 |
| | 5 | 0.08 | 0.09 | 0.16 | 0.60 | 0.45 | 0.42 |
| | 6 | 0.03 | 0.03 | 0.12 | 0.18 | 0.09 | 0.70 |
| W | 1 | 0.20 | 0.19 | 0.25 | 0.44 | 0.64 | 0.10 |
| | 2 | 0.13 | 0.16 | 0.18 | 0.39 | 0.62 | 0.21 |
| | 3 | 0.16 | 0.17 | 0.16 | 0.38 | 0.36 | 0.24 |
| | 4 | 0.19 | 0.20 | 0.26 | 1.14 | 0.34 | 0.82 |
| | 5 | 0.30 | 0.31 | 0.36 | 1.06 | 0.30 | 0.85 |
| | 6 | 0.13 | 0.13 | 0.17 | 0.59 | 0.12 | 0.77 |
| RMSE | 1 | 0.59 | 0.62 | 0.66 | 0.95 | 1.10 | 0.94 |
| | 2 | 0.53 | 0.51 | 0.53 | 0.79 | 1.05 | 1.27 |
| | 3 | 0.54 | 0.54 | 0.52 | 0.97 | 0.83 | 1.35 |
| | 4 | 0.55 | 0.60 | 0.75 | 1.38 | 1.06 | 1.59 |
| | 5 | 0.58 | 0.61 | 0.82 | 1.38 | 1.06 | 1.77 |
| | 6 | 0.30 | 0.31 | 0.61 | 0.79 | 0.72 | 1.56 |

Table 3: Median AREs for estimating HR, TTP, W and RMSE of the simulated HRFs from different methods.

three methods. Interestingly, the two spline methods lead to very similar results, possibly because Taylor expansion on $W$ can be effectively assimilated into the expansion on latency as both of them involve the term $f_k^{(1)}(t)$. The simulation also demonstrates that the two spline methods based on models (2) and (3) can well approximate the sixth HRFs even though the models do not exactly match the underlying truth.

AR (1) and i.i.d. errors were also simulated and the results were very similar to the above (thus omitted here), suggesting the proposed method is robust to the autocorrelation structure of the noise.

*3.2. Illustrative example*

**Subjects.** The data were collected during a study examining human social contact, attachment, and the social regulation of emotion (Coan et al., 2006; Coan, 2010; Coan, 2011; Coan, Beckes, and Allen, 2012). In total, 22 pairs of friends (11 male, 11 female) participated in exchange payment. Subjects were recruited from a larger representative longitudinal community sample (Allen et al., 2007). All participants were between 22 and 28 years of age at the time of participation, with 37% identified as black and 63% identified as white.

**Experimental Design.** One participant of each pair was threatened with mild electric shock during fMRI BOLD imaging while either holding the hand of a stranger, holding the hand of a friend, or holding no hand at all in three separate blocks. Each block − randomized within subjects − designed to test the neural response to threat during social contact with a familiar other, during social contact generally, and alone, respectively. Each block was composed of 24 trials half of which possessed a $20\%$ chance of shock and the other half were safe from the threat of shock. Threat cues (a red "X" on a black background) indicated a 20% likelihood of receiving an electric shock to the ankle−shock would accompany the end cue if delivered, and safety cues (a blue "O" against a black background) indicated no chance of shock. Each trial began with a threat or safety cue followed by a fixation cross during the resting period. The resting period lasted for 4-10 seconds (jittered cross trials), at which time an end cue would be presented for 1 second. Electric shocks were delivered using an isolated physiological stimulator (Coulbourn Instruments, Allentown, PA) with 1 second duration at 4 mA. All subjects received two shocks per block.

**Data Acquisition and Preprocessing.** A Siemens 3.0 Tesla MAGNETOM Trio high-speed magnetic imaging device at UVA's Fontaine Research Park, with a CP transmit/receive head coil with integrated mirror, was used to collect fMRIs. Two hundred twenty-three functional T2$^*$-weighted Echo Planar images (EPIs) sensitive to BOLD contrast were collected per block, in volumes of 28 3.5-mm transversal echo-planar slices (1-mm slice

gap) covering the whole brain (1-mm slice gap, TR=2000ms, TE=40ms, flip angle=90°, FOV= 192 mm, matrix= 64×64, voxel size= 3×3×3.5mm). Before functional scanning, 176 six high-resolution T1-magnetization-prepared rapid-acquisition gradient echo images were acquired to localize function (1-mm slices, TR=1900 ms, TE=2.53ms, flip angle= 9°, FOV=250mm, voxel size= 1×1×1mm).

| | | Threat % | | | Rest % | | |
|---|---|---|---|---|---|---|---|
| Comp. | FDR | dACC | OFC | Insula | dACC | OFC | Insula |
| Cond. | % | +/-⋆ | +/-⋆ | +/-⋆ | +/-⋆ | +/-⋆ | +/-⋆ |
| Alone | 5 | 22.7/5.9 | 11.8/2.8 | 21.1/2.9 | 42.1/0.7 | 24.3/1.4 | 28.8/4.8 |
| vs | 10 | 34.8/7.8 | 18.5/8.3 | 27.7/5.1 | 50.9/0.9 | 31.6/4.7 | 34.9/9.0 |
| Friend | 20 | 47.1/10.4 | 25.2/16.3 | 35.6/9.6 | 59.3/2.3 | 40.4/10.8 | 41.9/13.3 |
| Alone | 5 | 37.3/5.7 | 19.5/5.1 | 24.1/6.5 | 41.3/1.5 | 26.2/2.7 | 34.5/4.1 |
| vs | 10 | 45.8/7.8 | 27.3/10.3 | 31.7/12.8 | 48.5/2.5 | 34.4/7.0 | 41.2/7.4 |
| Stranger | 20 | 55.8/10.0 | 35.0/16.6 | 39.4/17.0 | 56.2/4.3 | 42.1/11.3 | 47.8/11.2 |
| Stranger | 5 | 2.8/12.6 | 6.4/9.9 | 17.0/11.4 | 11.9/9.6 | 11.3/10.2 | 16.9/22.4 |
| vs | 10 | 5.8/20.0 | 11.5/18.9 | 23.3/17.6 | 21.6/13.9 | 17.0/17.2 | 22.4/27.5 |
| Friend | 20 | 10.6/27.2 | 17.9/27.8 | 28.8/24.3 | 31.0/20.4 | 23.7/24.8 | 28.0/32.1 |

Table 4: The percentages of voxels in the ROIs selected by the spline method with different response magnitudes under different hand holding conditions after controlling for the FDR at 5%, 10%, and 20%, respectively. ⋆ The number before "/" is the percentage of voxels having larger magnitude under the first condition than that under the second condition; the number after "/" is the percentage of voxels having smaller magnitude under the first condition than that under the second condition.

Preprocessing was carried out via FMRIB's Software Library (FSL) software (Version 5.98; Smith et al., 2004; Woolrich et al., 2009). Motion correction was conducted via the Linear Image Registration Tool (MCFLIRT; Jenkinson et al., 2002) of FMRIB, with slice scan-time correction and high-pass filtering (100 second cutoff). BET (Smith, 2002) brain extraction was used to eliminate non-brain voxels, and a 5-mm full width at half maximum Gaussian kernel was used for smoothing. Registration of the images in FLIRT (Jenkinson et al., 2002) was based on Montreal Neurological Institute (MNI) space.

ROIs were determined structurally using the Harvard subcortical brain atlas, and were chosen for their likely involvement in affective processing based on previous studies (e.g., Knutson et al., 2000). The ROIs chosen for analysis were the dorsal anterior cingu-

late cortex (dACC), orbitofrontal cortex (OFC), and insula, regions that are commonly implicated in negative affect and threat responding.

Hand Holding with Friends

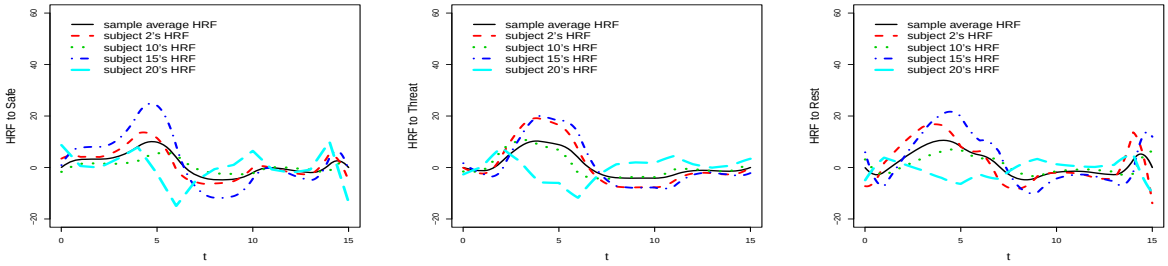


(a) HRF Safe (b) HRF Threat (c) HRF Rest

Alone

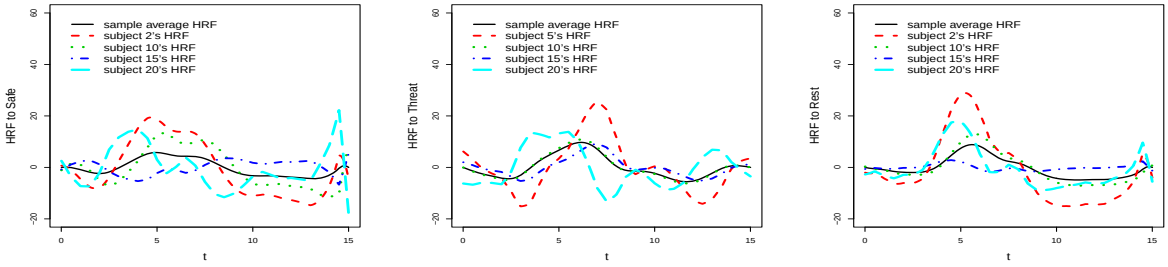


(d) HRF Safe (e) HRF Threat (f) HRF Rest

Figure 2: **Estimated $\hat{h}_{i,k}$ and $\hat{f}_k(t)$ for one selected voxel in dACC.** (a) HRFs in response to safety cue when hand holding with friends; (b) HRFs in response to threat cue when hand holding with friends; (c) HRFs at rest when hand holding with friends; (d) HRFs in response to safety cue when alone; (e) HRFs in response to threat cue when alone; (f) HRFs at rest when alone;

**Statistical Analysis and Discussion.** The proposed method was applied to the fMRI data from the three ROIs voxel by voxel. We included three stimuli – threat cue, safety cue, and rest period – in the GLM for each fMRI time series. To compare the brain activity responsive to the threat cue under different hand holding conditions, we first estimated the HRFs of the three stimuli for each subject and voxel by the spline method within each block independently, then extracted the HR estimates of the threat cue subtracted

by the HR estimate of the baseline safety cue, and conducted pairwise comparison of the resulting quantities under different hand holding conditions (alone, stranger, friend) using t-tests. Table 4 presents the percentages of the voxels in the three ROIs whose response magnitudes to the threat cue were identified to be different in the pairwise comparison of hand holding conditions, with the false discovery rate (FDR) controlled at 5%, 10%, and 20%, respectively. We used Benjamini-Hochberg (BH) threshold (Benjamini and Hochberg, 1995) based on the predetermined FDR for multiple hypothesis testing correction. Figure 2 shows the $\hat{h}_{i,k}(t)$ and $\hat{f}_k(t)$ estimated from the proposed approach for a representative voxel in dACC with a significant contrast between alone and hand-holding-with-friend conditions at rest. The pooled estimate $\hat{f}_k(t)$ clearly is much less variant and smoother compared to the individual HRF estimates. The upper panel in Figure 3 displays the heat maps of P-values in testing whether the response magnitudes of voxels in the three ROIs—dACC, OFC, and insula—to threat is greater under the alone condition than under the hand-holding-with-friend condition.

| | | Threat % | | | Rest % | | |
|---|---|---|---|---|---|---|---|
| Comp. Cond. | Method | dACC +/-$^\star$ | OFC +/-$^\star$ | Insula +/-$^\star$ | dACC +/-$^\star$ | OFC +/-$^\star$ | Insula +/-$^\star$ |
| Alone | Canonical | 0.1/0.7 | 0.1/1.1 | 0.0/0.8 | 0.1/0.0 | 0.1/0.8 | 0.0/0.5 |
| vs | Tik-GCV | 3.9/0.0 | 0.3/0.2 | 0.2/0.2 | 5.1/0.0 | 0.4/0.3 | 0.8/0.0 |
| Friend | SFIR | 0.1/1.6 | 0.5/1.0 | 0.2/2.5 | 0.2/0.3 | 0.3/0.8 | 0.0/2.0 |
| Alone | Canonical | 0.6/0.1 | 0.0/0.4 | 0.8/0.3 | 0.0/1.2 | 0.0/2.9 | 0.0/2.8 |
| vs | Tik-GCV | 4.7/0.1 | 0.7/0.2 | 4.9/0.2 | 1.6/0.1 | 0.9/0.6 | 0.8/0.1 |
| Stranger | SFIR | 0.1/1.5 | 0.1/1.3 | 0.2/1.3 | 1.2/0.3 | 0.4/0.5 | 1.0/1.0 |
| Stranger | Canonical | 0.1/0.7 | 0.3/0.8 | 0.1/1.7 | 0.8/0.0 | 2.1/0.0 | 0.7/0.0 |
| vs | Tik-GCV | 0.4/0.2 | 0.4/0.6 | 0.2/1.0 | 1.2/0.0 | 0.7/0.4 | 0.3/0.1 |
| Friend | SFIR | 0.3/0.2 | 0.7/0.4 | 0.2/0.5 | 0.2/1.1 | 0.2/0.7 | 0.2/2.4 |

Table 5: The percentages of ROI voxels identified by canonical, Tik-GCV, and SFIR methods with significantly different (at 1% significance level) response magnitudes to threat and rest period under different hand holding conditions. $^\star$ the number before "/" is the percentage of voxels having larger magnitude under the first condition than that under the second condition; the number after "/" is the percentage of voxels having smaller magnitude under the first condition than that under the second condition.

The data analysis shows that the number of voxels identified as more active was

greatest when subjects were alone and least when subjects were holding hands with a friend. These results are consistent with those reported by Coan, Beckes, and Allen (2012). Beckes and Coan (2011) provided an explanation through social baseline theory: because emotion regulation is an effortful and energy consuming activity, the human brain has evolved to "outsource" emotion regulation efforts to its social resources whenever possible—a strategy that leads humans to perceive the environment as less threatening when in close proximity to relational partners like friends and loved ones. Thus, people are less threat responsive and use fewer resources related to effortful self regulation when social support is available. Moreover, the relatively small difference between friend and stranger hand holding provides additional evidence that proximity to other humans (even strangers) is default or baseline regulatory strategy of the human brain.

Interestingly, we also found that the brain at "rest" is actually more active during the alone condition than during hand holding, as shown in the last three columns of Table 4 and the lower panel of Figure 3. Though this phenomenon has not been previously reported, it is likely that anticipatory anxiety builds over the resting period, diminishing either after the threat has been removed or the actual painful stimulus has been applied (e.g., Grillon et al., 2007). Thus, this effect is likely driven by the uncertainty participants are experiencing while alone in the scanner, even during the rest period.

We have also fitted three existing methods − SFIR, Tik-GCV, and the canonical method − to the data. Using the BH threshold with a relatively high level of FDR 20%, we found that the three methods failed to pick up any signal in any of the ROIs, with the percentage of selected voxels being 0 in most cases. To better illustrate, Table 5 instead presents the percentages of voxels whose response magnitudes during the threat and rest cues were identified to be significantly different under different hand holding conditions by the three methods using 1% significance level, without correction for multiple comparisons. It is striking that even here the percentages of selected voxels are much smaller than the nominal level in most cases. The poor performance of these methods is likely due to the large variances resulted from the low SNR of the data. This is not surprising given that

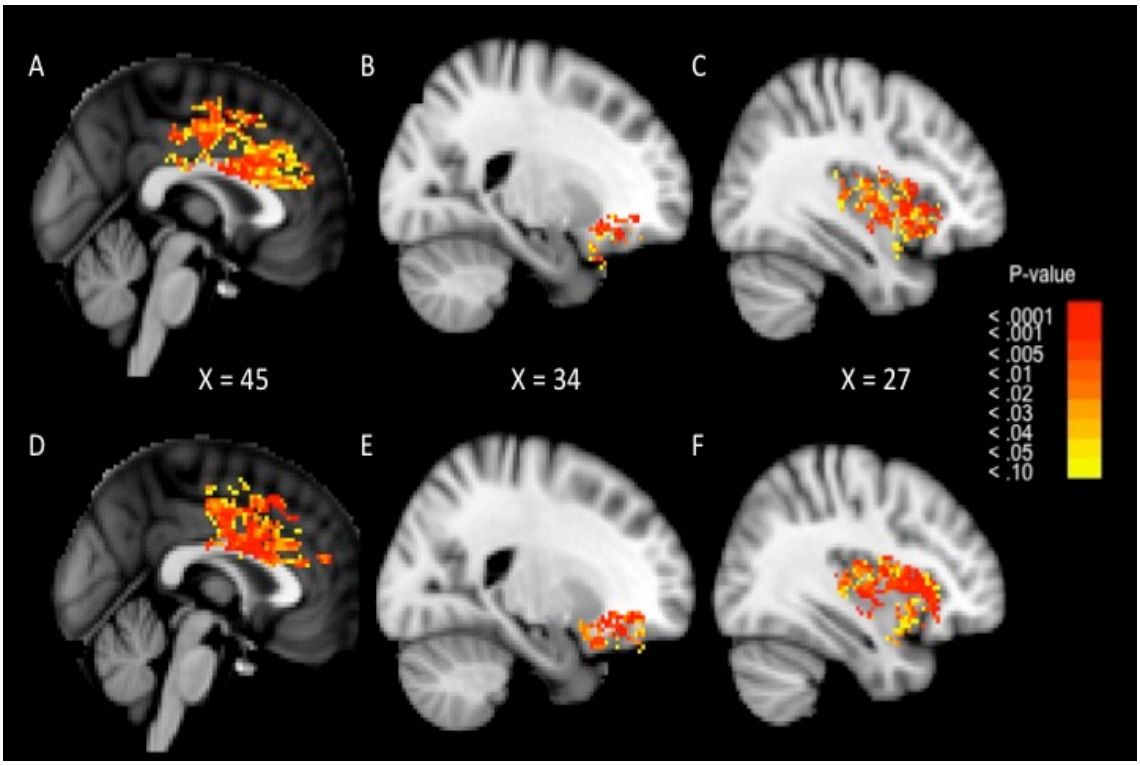


Figure 3: **Heat maps of significant voxels in ROIs.** (a) Voxels in dACC with larger response magnitudes to threat cue when alone than when holding hand with friends; (b) voxels in OFC with larger response magnitudes to threat cue when alone than when holding hand with friends; (c) voxels in insula with larger response magnitudes to threat cue when alone than when holding hand with friends; (d) voxels in dACC with larger response magnitudes during rest period when alone than when holding hand with friends; (e) voxels in OFC with larger response magnitudes during rest period when alone than when holding hand with friends; (f) voxels in insula with larger response magnitudes during rest period when alone than when holding hand with friends.

these methods do not take into account of the pooled sample information. Moreover, the results suggest that the canonical form may not fit the underlying HRFs well here. We acknowledge that the significant efficiency gain is obtained at the cost of a modest increase in computation. Specifically, for a ROI with around 6000 voxels, the spline method takes about 5 minutes using an R-2.15.2 program on a laptop computer with 2.50GHz CPU and 8GB memory, while the other three methods in comparison all take less than 40 seconds.

As pointed out by a reviewer, Figure 3 implies significant activation in the corpus callosum. Given the growing body of evidence on fMRI activation in white matter (Yarkoni

et al, 2009; Fraser et al, 2012), the proposed method may have captured the white matter HRF in a data-driven manner, and may have potential to be used for further investigations of white matter and gray matter HRFs.

## 4. Conclusion

Within the framework of the GLM, we proposed a new semi-parametric model that assumes the HRFs across subjects share a common functional shape, while accounting for subject-specific magnitudes and latencies. The nonparametric spline basis method was employed to construct the common functional shape to accommodate the variation of HRF shapes across different regions and stimuli. A fast-to-compute estimation strategy hinging on converting the resulting GLM to a bilinear model has been provided.

The main strength of the proposed approach lies in the simultaneous modelling of population-wide common properties and subject-specific characteristics of brain activity. The key assumption of subjects sharing a common functional shape of the HRF for a fixed voxel is plausible due to three properties of the HRFs: first, nearly all the HRFs in the literature adopt a single-mode shape; second, peaks of the HRFs usually occur between 5s and 8s; third, all the HRFs satisfy the boundary conditions, i.e., values of the HRF beyond the domain equal zero. These properties virtually guarantee that the HRFs have a similar basic shape, which enables us to "borrow" information across subjects and sharpen our analysis. For example, even though the SNR is usually low within each individual's data, stable and accurate estimates of the common HRF shape can be obtained by adding subjects. Moreover, once the common HRF shape is determined, the number of free parameters of the HRF for each combination of subjects and stimuli is reduced to two−HR and TTP −whose variation in the population is easier to detect than characteristics such as initial dip and undershoot. However, if the research target is to evaluate initial dip and undershoot−which have a complicated relationship with HR, TTP, and W−the proposed model (2) may not be delicate enough.

Our estimation relies on first-order Taylor expansion. Its accuracy depends on the closeness of the subject-specific latencies to zero. When there is considerable variation

in latency across subjects, setting latencies to zero in the estimation procedure would lead to results with a large bias. In such situations, with long enough observational time for each subject, using higher-order Taylor expansions and estimating the coefficients of the higher-order derivatives (instead of setting them to zero) can mitigate this problem. As long as the latency variation is within one experimental time unit, first-order Taylor expansion is expected to provide reasonable estimates.

We used penalized spline smoothing to approximate the shape of the HRFs, and the penalization parameter was chosen by minimizing the estimated AMSE. Generalized cross-validation (GCV) is an alternative computationally efficient method for parameter selection. The proposed algorithm and GCV have similar computational time, but they have different estimation targets: the former is focused on estimating population mean HRF, while the latter aims at obtaining the optimal parameter for estimating each individual subject's HRFs.

We note that the HR estimates from the spline methods are no longer independent across subjects, because the common HRF shape is estimated using all the data. This is not of great concern because variance in estimating a common HRF shape is generally small as long as the sample size is large enough. In fact, more uncertainty is attributed to estimating the subject-specific effects.

The spline method is developed for HRF estimation, and the resulting estimates from data with multiple stimuli may not be optimal for conducting hypothesis tests to identify voxels responsive to a specific stimulus, or voxels reacting differentially under different stimuli. This is because regularization can induce nonzero and unequal bias for the HRFs of different stimuli. The same issue arises in other regularization-based methods, such as SFIR and Tik-GCV. When the primary analysis goal is to identify active voxels in multi-stimulus data, the kernel-smoothed method proposed in Zhang et al. (2012) may be more suitable.

## Appendix

**Evaluation of AMSE of $\hat{a}_{l,k}$.** As the MSE of $\sum_{i=1}^{n} \hat{\eta}_i/n$ for each $i$ consists of bias and variance two parts:

$$\mathbb{E}(\sum_{i=1}^{n} \frac{\hat{\eta}_i}{n} - \sum_{i=1}^{n} \frac{\eta_i}{n})^2 = (\sum_{i=1}^{n} \frac{1}{n} \mathbb{E}(\hat{\eta}_i) - \sum_{i=1}^{n} \frac{\eta_i}{n})^2 + (\sum_{i=1}^{n} \frac{1}{n^2} \mathbb{V}(\hat{\eta}_i)), \tag{10}$$

we first derive the mean and variance of $\hat{\eta}_i$. Note that the expectation and variance are taken on every element of the vector. Under i.i.d. assumption of $\boldsymbol{\varepsilon}_i$ in model (7), the OLS estimate of $\eta_i$, $\hat{\eta}_i^{OLS} = (\Omega_0^i)^{-1}\Lambda_i' Y_i$, is an unbiased estimate of $\eta_i$ with variance $\sigma_i^2(\Omega_0^i)^{-1}$. Since $\hat{\eta}_i$ is linear of $\hat{\eta}_i^{OLS}$: $\hat{\eta}_i = (\Omega_\lambda^i)^{-1}\Omega_0^i\hat{\eta}_i^{OLS}$, we have the mean and variance of $\hat{\eta}_i$ as follows:

$$\mathbb{E}(\hat{\eta}_i) = (\Omega_\lambda^i)^{-1}\Omega_0^i\eta_i \quad \text{and} \quad \mathbb{V}(\hat{\eta}_i) = \sigma_i^2(\Omega_\lambda^i)^{-1}\Omega_0^i(\Omega_\lambda^i)^{-1}.$$

From above, the bias of $\hat{\eta}_i$ is given by $\left((\Omega_\lambda^i)^{-1}\Omega_0^i - \mathbf{I}_{3+K\cdot(L-2)}\right)\eta_i$, whose accurate estimate is difficult to obtain in practice due to small SNR of individual subject's data. Instead, we use sample-averaged estimate $\bar{\eta}_0$ (usually with a small variance and bias) to replace each $\eta_i$, leading to the bias estimate of $\sum_{i=1}^{n} \hat{\eta}_i/n$ as

$$\sum_{i=1}^{n} \left((\Omega_\lambda^i)^{-1}\Omega_0^i - \mathbf{I}_{3+K\cdot(L-2)}\right)\bar{\eta}_0/n. \tag{11}$$

For the variance part in (10), $\sigma_i^2$ can be evaluated by $\hat{\sigma}_i^2$. However, due to the large variation of $\sigma_i^2$ across subjects, we use median of $\hat{\sigma}_i^2$ to replace each $\sigma_i^2$ for robustness, and obtain the variance estimate of $\sum_{i=1}^{n} \hat{\eta}_i/n$ as

$$\sum_{i=1}^{n} \text{diag}\left((\Omega_\lambda^i)^{-1}\Omega_0^i(\Omega_\lambda^i)^{-1}\right)\hat{\sigma}^2/n^2. \tag{12}$$

Summing up the squared elements in (11) and elements in (12) excluding those corresponding to the drifting terms, we obtain the estimate of AMSE($\lambda$).

**Acknowledgments**

T. Zhang's research is partially funded by the DMS grant 12-09118 of the U.S. NSF. F. Li's research is partially funded by the DMS grant 12-08983 of the U.S. NSF. Part of the project was conducted when Zhang and Li were research fellows of the Object Data Analysis program of the U.S. Statistical and Applied Mathematical Sciences Institute (SAMSI). J. Coan's research was partially funded by a grant issued by the National Institute of Mental Health (NIMH). The project described was supported by Award Number R01MH080725 to Coan. The content is solely the responsibility of the authors and does not necessarily represent the official views of NIMH, the National Institutes of Health or SAMSI. We thank the editor and two reviewers for comments. Support from Casey Brown, Karen Hasselmo, Alexander Tatum, and Zoe Englander is also acknowledged.

[1] Aguirre, G.K., Zarahn, E. and D'Esposito, M. (1998). The variability of human, BOLD hemodynamic responses. *NeuroImage* **8**, 360-369.

[2] Allen, J. P., Porter, M., McFarland, F. C., McElhaney, K. B., Marsh, P. (2007). The relation of attachment security to adolescents' paternal and peer relationships, depression, and externalizing behavior. *Child Development* **78**, 1222-1239.

[3] Beckes, L. and Coan, J. A. (2011). Social baseline theory: The role of social proximity in emotion and economy of action. *Social and Personality Psychology Compass* **5**, 976-988.

[4] Benjamini, Y. and Hochberg, Y. (1995). Controlling the false discovery rate: a practical and powerful approach to multiple testing. *Journal of the Royal Statistical Society, Ser. B* **57(1)**, 289-300.

[5] Brosch, J., Talavage, T., Ulmer, J., and Nyenhuis, J. (2002). Simulation of human respiration in fMRI with a mechanical model. *IEEE Transcations on Biomedical Engeering* **49**, 700-707.

[6] Buxton, R. B., Uludag, K., Dubowitz, D. J., and Liu, T. T. (2004). Modeling the hemodynamic response to brain activation. *NeuroImage* **23**, 220-233.

[7] Casanova, R., Ryali, S., Serences, J., Yang, L., Kraft, R., Laurienti, P. J., Maldjian, J. A. (2008). The impact of temporal regularization on estimates of the BOLD hemodynamic response function: a comparative analysis. *NeuroImage* **40(4)**, 1606-18.

[8] Casanova, R., Yang, L., Hairston, W. D., Laurienti, P. J., Maldjian, J. A. (2009). Evaluating the impact of spatio-temporal smoothness constraints on the BOLD hemodynamic response function estimation: an analysis based on Tikhonov regularization. *Physiological Measurement* **30(5)**, N37-51.

[9] Coan, J. A. (2010) Adult attachment and the brain. *Journal of Social and Personal Relationships*, **27**: 210-217.

[10] Coan, J. A. (2011) The social regulation of emotion. In *Oxford Handbook of Social Neuroscience*, pp. 614-623. New York, Oxford University Press.

[11] Coan, J.A., Beckes, L., and Allen, J.P. (2012). Childhood maternal support and neighborhood quality moderate the social regulation of neural threat responding in adulthood. *International Journal of Psychophysiology*.

[12] Coan, J. A., Schaefer, H. S., and Davidson, R. J. (2006). Lending a hand: Social regulation of the neural response to threat. *Psychological Science*, **17**: 1032-1039.

[13] Crainiceanu, C. M., Staicu, A., and Di, C. (2009). Generalized Multilevel Functional Regression. *Journal of the American Statistical Association* **104**, 1550-1561.

[14] Dale, A. (1999) Optimal Experimental Design for Event-Related fMRI. *Human Brain Mapping*, **8**, 109-114.

[15] De Boor, C. (2001). *A Practical Guide to Splines (Revised Edition)*. Springer.

[16] Di, C., Crainiceanu, C. M., Caffo, B. S., and Punjabi, N. M. (2009) Multilevel functional principal component analysis. *Annals of Applied Statistics* **3**, 458-488.

[17] Eubank, R. L. (1988). *Spline Smoothing and Nonparametric Regression*. Marcel Dekker, Inc., New York.

[18] Fraser, L. M., Stevens, M. T., Steven, D. B., and D'Arch, R. CN. (2012). White versus gray matter: fMRI hemodynamic responses show similar characteristics, but differ in peak amplitude. *BMC Neuroscience*, **13**: 91.

[19] Friston, K. J., Fletcher, P., Josephs, O., Holmes, A., Rugg, M. D., and Turner, R. (1998). Event-related fMRI: characterizing Differential Responses. *NeuroImage* **7**, 30-40.

[20] Friston, K. J., Holmes, A.P., Price, C. J., Büchel, C., and Worsley, J.K. (1999). Multi-subject fMRI Studies and Conjunction Analyses. *NeuroImage* **10**, 385-396.

[21] Friston, K. J., Jezzard, P. J., and Turner R. (1994). Analysis of functional MRI time-series. *Human Brain Mapping* **1**, 153-171.

[22] Friston, K. J., Holmes, A. P., Poline, J. B., Grasby, P. J., Williams, S. C., Frackowiak, R.S. and Turner, R. (1995a). Analysis of fMRI time-series revisited. *NeuroImage* **2**, 45-53.

[23] Friston, K. J., Holmes, A. P., Worsley, K., Poline, P. J., Frith, C. and Frackowiak, R. (1995b). Statistical parametric maps in functional imaging: A general linear approach. *Human Brain Mapping* **2**, 189-210.

[24] Glover, G. H. (1999). Deconvolution of impulse response in event-related BOLD fMRI. *NeuroImage* **9**, 416-429.

[25] Goutte, C., Nielsen, F. A., and Hansen, L. K. (2000). Modeling the haemodynamic response in fMRI using smooth FIR filters. *IEEE Transactions on Medical Imaging* **19**, 1188-1201.

[26] Green, P. J. and Silverman, B. W. (1994). *Nonparametric Regression and Generalized Linear Models*. CRC Press.

[27] Grillon, C., Ameli, R., Merikangas, K., Woods, S. W., and Davis, M. (2007). Measuring the time course of anticipatory anxiety using the threat potentiated startle reflex. *Psychophysiology* **30**, 340-346.

[28] Handwerker DA, Ollinger JM, D'Esposito M. (2004). Variation of BOLD hemodynamic responses across subjects and brain regions and their effects on statistical analyses. *NeuroImage* **21**, 1639-51.

[29] Henson, R., Price, C. J., Rugg, M. D., Turner, R., and Friston, K. J. (2002). Detecting latency differences in event-related BOLD responses: application to words versus nonwords and initial versus repeated face presentations. *NeuroImage* **15**, 83-97.

[30] Jenkinson, M., Bannister, P., Brady, M., and Smith, S. (2002). Improved optimization for the robust and accurate linear registration and motion correction of brain images. *NeuroImage* **17**, 825-41.

[31] Knutson, B., Westdorp, A., Kaiser, E., and Hommer, D. (2000). FMRI visualization of brain activity during a monetary incentive delay task. *NeuroImage* **12**, 20-27.

[32] Ladd, W., and Lindstrom, M. (2000). Self modeling for two-dimensional response curves. *Biometrics*, **56**, 89-97.

[33] Lange, N., Strother, S. C., Anderson, J. R., Nielsen, F. A., Holmes, A. P., Kolenda, T., Savoy, R., and Hansen, L. K. (1999). Plurality and resemblance in fMRI data analysis. *NeuroImage* **10**, 282-303.

[34] Li, Y., Wang, N., and Carroll, R. J. (2010). Generalized Functional Linear Models with Semiparametric Single-Index Interactions. *Journal of the American Statistical Association* **105**, 621-633.

[35] Liao, C. H., Worsley, K. J., Poline, J-B., Aston, J. A. D., Duncan, G. H., and Evans, A. C. (2002). Estimating the Delay of the fMRI response. *NeuroImage* **16**, 593-606.

[36] Lindquist, M. A. and Wager, T. D. (2007). Validity and power in hemodynamic response modelling: a comparison study and a new approach. *Human Brain Mapping* **28**, 764-784.

[37] Lindstrom, M. (1995). Self modeling with random scale and shift parameters and a free-knot spline shape function. *Statistics in Medicine*, **14**, 2009-2021.

[38] Luo, H. and Puthusserypady, S. (2008). Analysis of fMRI Data With Drift: Modified General Linear Model and Bayesian Estimator. *IEEE Transcations on Biomedical Engeering* **55**, 1504-1511.

[39] Marrelec, G., Benali, H., Ciuciu, P., Pelegrini-Issac, M., Poline, J. B. (2003). Robust Estimation of the Hemodynamic Response Function in Event-Related BOLD fMRI Using Basic Physiological Information. *Human Brain Mapping* **19**, 1-17.

[40] Marrelec, G., Benali, H., Ciuciu, P., and Poline, J. B. (2001). Bayesian estimation of the hemodynamic of the hemodynamic response function in functional MRI. *AIP Conference Proceedings* **617**, 229-247.

[41] Müller, H. and Stadtmüller, U. (2005). Generalized functional linear models. *Annals of Statistics* **33**, 774- 805.

[42] Mumford, J. A. and Nichols, T. E. (2006). Modeling and Inference of Multisubject fMRI Data. *IEEE Engineering in Medicine and Biology Magazine*, **25(2)**, 42-51.

[43] Ogawa, S., Tank, D.W., Menon, R., Ellerman, J.M., Kim, S.G., Merkle, H., Ugurbil, K. (1992). Intrinsic signal changes accompanying sensory simulation: functional brain mapping and magnetic resonance imaging. *Proc. Natl. Acad. Sci.* **89**, 5951-5955.

[44] Ollinger, J. M., Corbetta, M., and Shulman, G. L. (2001). Separating processes within a trial in event-related functional MRI. *NeuroImage* **13** 218-229.

[45] Parker, R. L., and Rice, J. A. (1985). Discussion of "Some Aspects of the Spline Smoothing Approach to Nonparametric Regression Curve Fitting" by B. W. Silverman. *Journal of the Royal Statistical Society, Ser. B*, **47**, 4042.

[46] Ramsay, J.O. and Silverman, B.W. (2005). *Functional data analysis, second edition*. Springer.

[47] Reiss, P. T. and Ogden, R. T. (2007) Functional principal component regression and functional partial least squares. *Journal of the American Statistical Association*, **102**, 984-996.

[48] Reiss, P. T. and Ogden, R. T. (2009) Smoothing parameter selection for a class of semiparametric linear models. *Journal of the Royal Statistical Society, Ser. B*, **71**, 505-523.

[49] Riera, J. J., Watanabe, J., Kazuki, I., Naoki, M., Aubert, E., Ozaki, T., and Kawashima, R. (2004). A state-space model of the hemodynamic approach: Nonlinear filtering of bold signals. *NeuroImage* **21**, 547-567.

[50] Ruppert, D., Wand, M. P., and Carroll, R. J. (2003). Semiparametric Regression. Cambridge University Press.

[51] Smith, A., Lewis, B., Ruttinmann, U., et al. (1999). Investigation of low frequency drift in fMRI signal, *NeuroImage* **9**, 526-533.

[52] Smith. S.M. (2002). Fast robust automated brain extraction. *Human Brain Mapping*, **17**, 143-155.

[53] Smith, S.M., Jenkinson, M., Woolrich, M.W., Beckmann, C.F., Behrens, T.E.J., Johansen-Berg, H., Bannister, P.R., De Luca, M., Drobnjak, I., Flitney, D.E., Niazy, R., Saunders, J., Vickers, J., Zhang, Y., De Stefano, N., Brady, J.M., and Matthews, P.M. (2004). Advances in functional and structural MR image analysis and implementation as FSL. Neuroimage 23(S1), 208-219.

[54] Vakorin, V. A., Borowsky, R., and Sarty, G. E. (2007). Characterizing the functional MRI response using Tikhonov regularization. *Statistics in Medicine* **26(21)**, 3830-3844.

[55] Wahba, G. (1990). *Spline Models for Observational Data*. Philadelphia: SIAM.

[56] Wood, S. N. (2011). Fast stable restricted maximum likelihood and marginal likelihood estimation of semiparametric generalized linear models. *Journal of the Royal Statistical Society, Ser. B*, **73**, 3-36.

[57] Woolrich, M. W., Behrens, T.E., and Smith, S.M. (2004). Constrained linear basis sets for HRF modelling using Variational Bayes. *NeuroImage* **21**, 1748-1761.

[58] Woolrich, M.W., Jbabdi, S., Patenaude, B., Chappell, M., Makni, S., Behrens, T., Beckmann, C., Jenkinson, M., and Smith, S.M. (2009). Bayesian analysis of neuroimaging data in FSL. *NeuroImage* **45**, S173-186.

[59] Worsley, K. J. and Friston, K.J. (1995). Analysis of fMRI time-series revisited again. *NeuroImage* **2**, 173-181.

[60] Worsley, K. J., Liao, C. H., Aston, J., Petre, V., Duncan, G. H., Morales, F., and Evans, A. (2002). A General Statistical Analysis for fMRI Data. *NeuroImage* **15**, 1-15.

[61] Yao, F., Müller, H., and Wang, J.(2005). Functional data analysis for sparse longitudinal data. *Journal of the American Statistical Association*, **100**, 577-590.

[62] Yarkoni, T., Barch, D. M., Gray, J. R., Conturo, T. E., and Braver, T. S. (2009). BOLD correlates of trial-by-trial reaction time variability in gray and white matter: a multi-study fMRI analysis. *PLoS ONE*, **4**, e4527.

[63] Zarahn, E. (2002). Using larger dimensional signal subspaces to increase sensitivity in fMRI time series analyses. *Human Brain Mapping* **17**, 13-16.

[64] Zhang, C. M., Jiang, Y. and Yu, T. (2007). A comparative study of one-level and two-level semiparametric estimation of hemodynamic response function for fMRI data. *Statistics in Medicine* **26**, 3845-61.

[65] Zhang, T., Li, F., Beckes, L., Brown, C., and Coan, J.A. (2012). Nonparametric inference of hemodynamic response for multi-subject fMRI data. *NeuroImage* **63**, 1754-1765.